



Article

Robotic Path Planning for Rice Seeding in Hilly Terraced Fields

Wenwu Yang ^{1,2,3,*}, Congquan Gong ¹, Xilin Luo ¹, Yong Zhong ¹, Ennan Cui ¹, Jianhao Hu ¹, Shiyu Song ¹, Haoyang Xie ¹ and Weiman Chen ¹

¹ Key Laboratory of Key Technology on Agricultural Machine and Equipment, Ministry of Education, College of Engineering, South China Agricultural University, Guangzhou 510642, China

² Maoming Branch, Guangdong Laboratory for Modern Agriculture, Maoming 525000, China

³ Huangpu Innovation Research Institute, South China Agricultural University, Guangzhou 510030, China

* Correspondence: yangwenwu@scau.edu.cn; Tel.: +86-15920498242

Abstract: To realize the autonomous operation of a terraced rice sowing robot, a set of sowing robot operation path planning algorithms with universal significance for small, irregular terraced plots is proposed. According to the characteristics of terraces and the agronomic requirements of sowing seeding, the operation path mainly includes parallel operation and boundaries surrounding the operation path. The boundary pre-collision detection method is expounded, and the cyclic detection method judges the U-turn area. The Bézier curve fitting algorithm was used to smooth the boundary wrapping path. To verify the feasibility of the algorithm, four typical irregular small fields located in 666.7-hectare terraces of Sama in Hong He Prefecture, Yunnan Province, were randomly selected, and a field map was obtained through Google Earth. An existing seeding robot was used as a model, and the simulation and comparison tests were carried out with the mainstream EHNS algorithm and boundary polyline algorithm under the ROS-kinetic platform in the Cen Village Scientific Research Base of South China Agricultural University. The actual boundaries of the four fields with the same simulation test were used as the map to verify the field experiment. The simulation test results show that the area coverage of the sowing operation is greater than 93.53% and the replay rate is less than 3.46%, and the field test results show that the area coverage of the sowing operation is greater than 94.33% and the replay rate is less than 3.03%. The simulation test is in good agreement with the field test results, indicating that the algorithm has good adaptability, which meets the requirements of a sowing robot for sowing operation path planning and can provide a certain reference for the path planning of irregular field operation robots in hilly and mountainous areas.



Citation: Yang, W.; Gong, C.; Luo, X.; Zhong, Y.; Cui, E.; Hu, J.; Song, S.; Xie, H.; Chen, W. Robotic Path Planning for Rice Seeding in Hilly Terraced Fields. *Agronomy* **2023**, *13*, 380. <https://doi.org/10.3390/agronomy13020380>

Academic Editor: Simon Pearson

Received: 26 December 2022

Revised: 14 January 2023

Accepted: 26 January 2023

Published: 28 January 2023



Copyright: © 2023 by the authors. Licensee MDPI, Basel, Switzerland. This article is an open access article distributed under the terms and conditions of the Creative Commons Attribution (CC BY) license (<https://creativecommons.org/licenses/by/4.0/>).

1. Introduction

The southern hilly and mountainous areas are an important grain production base in China, of which the rice planting area accounts for more than 60% of the total rice planting area in the country and plays an important role in national grain production. However, affected by factors such as geographical conditions, farming systems, and planting scale, mechanization in hilly and mountainous areas is still in its infancy, and there is a big gap with the national average. Therefore, vigorously developing agricultural mechanization in hilly and mountainous areas and improving the production capacity of rice mechanization is of great strategic significance for promoting agriculture and rural revitalization in mountainous areas [1–6].

Agricultural robots are one of the main directions for modern agricultural mechanization in hilly and mountainous areas, and many scientific research institutions at home and abroad have made outstanding contributions in the field of agricultural robot research [7–9]. Panasonic Corporation of Japan has developed a greenhouse tomato single-fruit picking robot that uses a camera and a distance image sensor to detect the distribution of plants and fruits in the area to be harvested [10]. Research institutes at the University of Bremen

in Germany have developed a selective harvesting robot for green asparagus that can be driven along asparagus dams in a field, detect asparagus stems, and determine which stems can be harvested [11]. The Korea Institute of Electronics and Communications Science has designed an agricultural robot capable of object detection [12]. Luo Xiwen's team from South China Agricultural University conducted research on the autonomous driving technology of agricultural machinery and realized the automatic driving of a rice direct broadcast machine and a paddy field sprayer [13]. Li Wei's team from China Agricultural University developed a cucumber-picking robot that can autonomously navigate movement in an unstructured environment and the visual system can effectively identify and locate fruits [14]. Niu Runxin from the Hefei Institute of Physical Sciences, Chinese Academy of Sciences, proposed a lidar-based trunk detection algorithm for the problem that slopes and weeds in orchards in hilly and mountainous areas affect the detection accuracy of fruit trees [15]. In recent years, many enterprises at home and abroad have begun to develop micro-small intelligent agricultural machinery equipment, which has better adaptability and a higher degree of automation than traditional machinery. However, due to short research and development times, late starts, and relatively immature technology, it is still in its infancy and has not been widely promoted and applied. Therefore, the research and development of agricultural robots with a small size and a high degree of intelligence is of great significance to promote the development of agricultural mechanization in hilly and mountainous areas [16].

Navigation, detection, action, and mapping are the four most important automation features of autonomous farming robots. Navigation is critical, and detection and mapping are often used. Path planning is the most important part of agricultural robot navigation and plays a “decision-making” role in the operation process of agricultural robots. Most of the operation paths of agricultural robots require full coverage path planning, and the evaluation indicators of the operation path include operation efficiency, energy consumption, operation conditions, etc., so that the advantages and disadvantages of the path can be judged together [17–20]. Utamima et al. proposed an evolutionary hybrid neighborhood search (EHNS) path optimization method for rectangular and non-convex polygon fields [21]. Oksanen and Visala et al. proposed a job path generation algorithm based on polygon-based trapezoidal decomposition [22]. The research team of the University of Messina in Italy proposed to find the optimal path between the two points of an unmanned intervention robot without collision by using the incremental gray wolf optimization algorithm (I-GWO) and the extended gray wolf optimization algorithm (EX-GWO) in farmland with the lowest processing costs and the most effective resource utilization [23]. The research team of the Institute of Technology of Aalto University in Finland proposed a greedy algorithm that can effectively solve the problem of optimal driving direction and subfield selection [24]. Based on the constraints of multiple vehicle turning modes and agricultural plots, the research team of Shanghai Jiao Tong University in China proposed a mixed rule path planning method based on the simulated annealing method [25]. To realize the remote scheduling and management of multi-machine collaborative navigation operations in the farmland operation environment, Cao Ruyue carried out research on global path planning based on the improved A* algorithm and the Bézier curve [26]. Huang Xiaomao proposed a set of rapeseed joint live broadcast operation path planning algorithms with universal significance for convex polygon boundary fields [27].

In summary, most of the current path planning research focuses on regular large field blocks, but there are a few studies on the path planning of irregular terraces in hills. Due to the poor natural endowment of hilly mountainous areas and the small and scattered plots of land, the degree of agricultural mechanization of rice cultivation has been difficult to improve. After recent years of exploration, agricultural robots can be used as a research direction to solve low mechanization rates in hilly and mountainous areas, and path planning is the decision-making system of agricultural robots, which puts forward specific requirements in the production process, so research that can be adapted to the path planning of seeding robots in hilly mountainous areas has considerable significance and

can also provide a certain reference for improving the level of agricultural mechanization in hilly and mountainous areas.

In this paper, aimed at the problems of low coverage and the high replay rate of traditional rice live path planning, path planning of seeding robots in hilly mountainous areas based on cyclic detection, pre-collision detection, curve fitting, and loop detection is proposed, and the corresponding optimization is made around the operation path at the boundary, which can provide important path parameter support for the subsequent navigation operation of seeding robots.

2. Materials and Methods

2.1. Operation Characteristics and Path Planning Requirements of the Terraced Rice Seeding Robot

Due to small field areas, irregularity and large drops are typical characteristics of hilly terraces; it is difficult to promote the application of agricultural machinery and equipment in the current market in hilly terraces, and rice planting in hilly terraces is still mainly artificial planting. To solve the problem of rice planting in terraced fields, this research group designed a micro electric seeding robot based on Songling SCOUT2.0 chassis; the schematic diagram of the robot architecture is shown in Figure 1, and the physical parameters of the robot are shown in Table 1. During the sowing operation, with the travel of the micro chassis, the seeding device carries out synchronous ditching, ridge, and seeding processes. When the ground turns, the seeding device is lifted away from the mud surface and the seeding is stopped. Since most of the hilly terraced boundaries are irregular curves, to ensure the coverage and replay rate of the seeding, the operation path of the seeding robot should be reasonably planned.

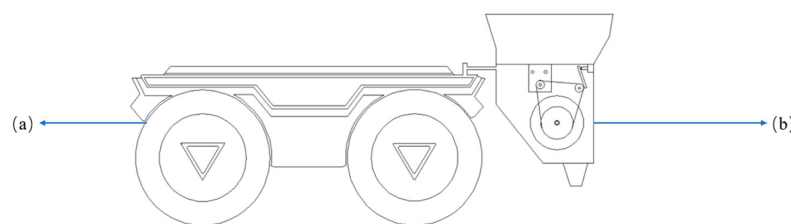


Figure 1. The schematic diagram of the robot architecture. (a) Robot chassis and (b) working device.

Table 1. Physical parameters of the seeding robot.

Project	Index
Length × height × width (mm)	930 × 699 × 348
Wheelbase (mm)	498
Body weight (Kg)	62
Steering mode	Four-wheel differential steering
Maximum speed (m/s)	1.5
Maximum climbing capacity (°)	30

Considering the ground curvature and field boundary combined with the agronomic requirements of rice planting, the planned sowing operation path has the following requirements:

- The operation path of the seeding robot should adapt to the requirements of terraced field seeding, e.g., different areas, shapes, and boundaries where the robot chassis planting device will operate.
- The working field should be covered globally and only once.
- The effective operation path is planned by the principle of “an internal parallel operation path and an external smooth operation path”.
- The seeding operation path can adapt to the operation parameters and characteristics of the seeding robot and minimize the turning area.
- Reduce the secondary rolling of the sowing area and reduce the repetition rate and missed rate.
- The algorithm should run stably and efficiently, and it should be highly adaptable to irregular boundary fields.

2.2. Algorithm Flow and Data Definition

For irregular boundary fields such as terraces, polygons or fitting curves are used to represent the actual boundary of the field, and the working plots are selected by a hand-held GPS manual dotting or GIS system, and each boundary point is stored in the reverse clockwise direction. Taking the boundary of the proposed operation field and the robot operation parameters as the input and the path point of the operation as the output, the algorithm flow of the seeding robot operation path is shown in Figure 2. The algorithm process mainly includes two parts: farmland information processing and path planning. The farmland information processing part is to generate key contour parameters and the robot coordinate system based on farmland information such as plot contour mapping point data. The path planning part calculates the set of path points including command information based on the operation parameters such as the operation direction, work width, robot radius, and starting orientation.

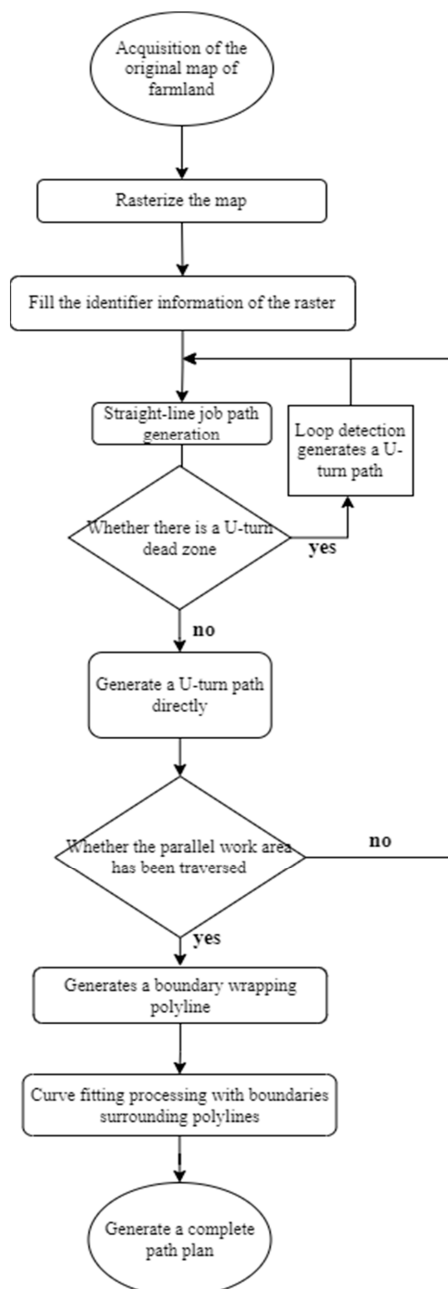


Figure 2. Algorithm flowchart.

The algorithm is mainly used for the planning of the effective operation path and turning path of the seeding robot. The effective operation path includes a parallel operation path and boundary surround operation path, and the algorithm generation principle involves raster map analysis, a collisional detection algorithm, a polyline algorithm, and a curve fitting algorithm. The turning path is a non-operation path when the robot turns around and changes the operation line, and the chassis of the seeding robot adopts the four-wheel differential in situ steering method, and it is also necessary to avoid the dead zone of the U-turn. To reduce the number of corners, the terraced boundary should be smoothed to ensure the smoothness of the operation path and improve the quality of the boundary surrounding the seeding operation.

2.3. Principle of Raster Map Generation

2.3.1. Map Rasterization

The map is first imported into the ROS-kinetic system for further processing. Then, the preset resolution of the map is entered. ROS-kinetic is used to obtain the number of rows and columns of the coordinate system map; it is also used to input the working width and radius information of the seeding robot. The following equation is used to calculate the size of grid L_{sg} shown in Equation (1):

$$L_{sg} = d_{\max}(\text{working width}/\text{resolution of map}, 1) \quad (1)$$

The function d_{\max} in Equation (1) returns the largest integer value.

Next, we input the coordinates of the starting point, rasterize the coordinates of the starting point, and obtain the rasterized coordinates of the starting point.

2.3.2. Raster Map Generation

Through raster analysis of a coordinate system map, parameters such as the row number, column number, grid size, and boundary-free grid size are obtained by using the preparation work carried out before rasterization, which is convenient for rasterization later. The preparatory work mainly uses the outer circle size of the robot to determine the grid size, the length and width of the map are divided by the grid size to calculate the row number and column number, and the boundary-free grid size is determined by the minimum turning radius of the robot. First, the center coordinate of each grid is set as the rectangular coordinate of the grid; then, each grid number corresponds to its rectangular coordinate one by one. The mapping relationship between any point (x, y) in the map and grid number N is shown in Equation (2).

$$N = \text{INT}(x/L_{sg}) + L/L_{sg} * \text{INT}(y/L_{sg}) \quad (2)$$

In Equation (2), L represents the spare size of the Yan farmland boundary, L_{sg} represents the grid size, and INT represents the round operation.

Similarly, the central coordinate of a single grid can also be calculated from the ordinary method; so, the mapping relationship between the central coordinate of the grid (X_g, Y_g) and the grid number N is shown in Equations (3) and (4):

$$X_g = (N \% M) * L_{sg} + L_{sg}/2 \quad (3)$$

$$Y_g = \text{INT}(N/M) * L_{sg} + L_{sg}/2 \quad (4)$$

In Equations (3) and (4), the $M = \text{INT}(\frac{L}{L_{sg}}) + 1$. The symbol $\%$ is a remainder operation.

The mapping relation and equation are used to parse the coordinate system map. The data extracted from the grid are compared to the initial value of the grid. If the value is greater than the initial value of the grid, then the grid has been occupied and the occupation identifier is 1. If the data in the grid are less than or equal to the initial value of the grid, then the grid is not occupied, and the occupation identifier is 0. In this way, each grid has

an occupation identifier (occupation identifier 1 means occupied, and occupation identifier 0 means idle) and the rasterization process of the map is completed. The rasterization process of the map is shown in Figure 3.

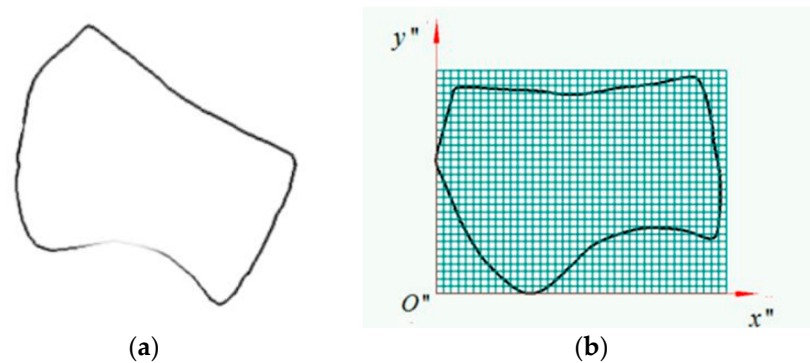


Figure 3. The rasterization processes. (a) Before the map is rasterized and (b) after the map is rasterized.

2.4. Generation of Parallel Job Paths

The selection of the operation direction should consider the direction with the highest operation coverage. Generally, the operation direction is obtained by the maximum span. The generation of parallel operation paths is based on the selected operation direction. If the map boundary is directly in front of the path direction (i.e., the occupation identifier of the identified grid is 1), the operation path is immediately set and the turning action is started. If the front grid is free (i.e., the occupation identifier of the grid is identified as 0), the job path is generated forward. After completing the turning action, we continue to generate the parallel operation path of the next line and repeat the cycle until the parallel operation area of the map is traversed and the generation of the entire parallel operation path is completed. The schematic diagram of parallel operation path generation is shown in Figure 4.

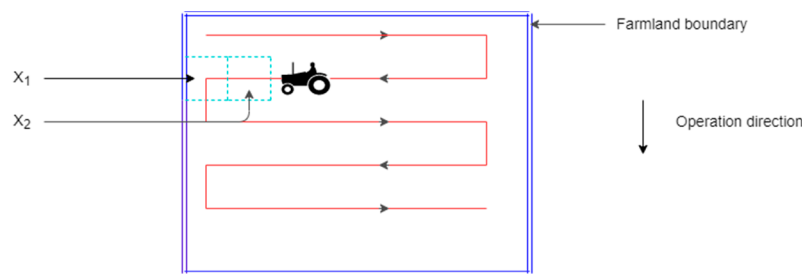


Figure 4. Schematic diagram of parallel work path generation. X_1 is the front grid that reminds you where to turn; X_2 is an empty position in the front grid.

2.5. Selection and Generation of Parallel Operation Path Turns

2.5.1. Way of Turning

The turning mode of the parallel working path is mainly based on right-angle turning, the chassis of the seeding robot in hilly and mountainous areas adopts a four-wheel differential chassis, and the turning method mainly turns with its geometric center as the center of rotation, which can minimize the influence of chassis length on the working width when turning, and the four-wheel differential steering is shown in Figure 5.

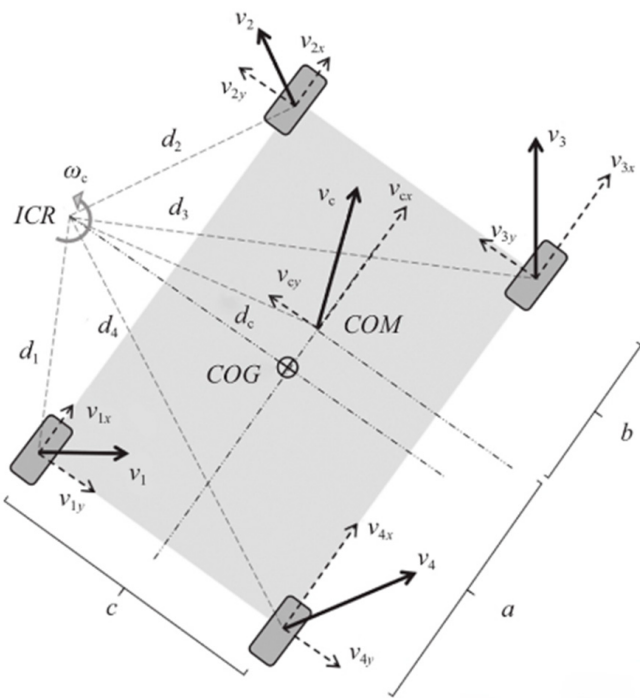


Figure 5. Four-wheel differential model. **ICR** is the rotate center; **COG** is the geometric center; d_i is the distance from the four wheels to the ICR; **COM** defines the centroid; d_c is the distance from COM to the ICR; c is the wheelbase of the left wheel to the right wheel; a is the distance from COM to the backend; and b is the distance from COM to the front end.

2.5.2. Judgment and Calculation of Turning Radius

Because in the parallel operation path the main way is to turn in situ, the determinants of the turning radius are therefore the working width L_f of the robot, and the minimum turning radius R_{\min} . The calculation is shown in Equation (5):

$$R_{\min} = L_f / 2 \quad (5)$$

Through the size conversion, it is converted to the minimum number of grids required S_{\min} , as shown in Equation (6):

$$S_{\min} = \text{INT}(R_{\min} / L_{sg}) \quad (6)$$

According to the above equation, the number of grids required by the current steering of the seeding robot can be obtained. When generating parallel operating paths, free grids of appropriate length can be set aside for turning.

2.5.3. Turn Dead Zone Loop Detection Judgment and Calculation of Turning Radius

Due to the irregular boundary of the field, it is necessary to avoid a normal U-turn at the boundary. During detection, identifier 1 is used when traveling in the same direction and then turning on the side of the grid. If identifier 1 is used, the current direction of the same side of the grid and assignments tailored for the boundary grid are there. If the vehicle needs to go back to detect and operate the direction of the same side of the grid, then the identifier is 0. The current grid will complete a turn cycle to detect the dead area. Figure 6 shows the schematic diagram of the U-turn dead zone judgment.

2.6. Generation and Processing of Boundary Surround Job Paths

Since seeding cannot be carried out in the right-angle turning area in the parallel operation area, resulting in the formation of missing seeds in the right-angle turning area, it is necessary to use the boundary around the operation path to reseed the area. However,

the boundary of the plot is irregular, and it is also necessary to sow the vacant area of the plot boundary to ensure maximum sowing coverage; therefore, it is wrapped and seeded using a boundary wrap-around job path to reduce the missed rate.

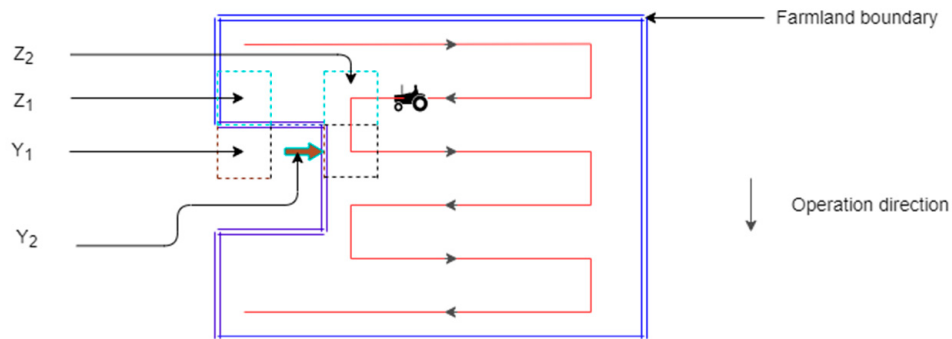


Figure 6. U-turn dead zone judgment diagram. Y_1 is the grid on the same side as the working direction; Y_2 is the detection direction on the same side as the working direction; Z_1 is the original turn; and Z_2 is the actual turn. If the U-turn dead zone judgment is not performed, the robot stops seeding at Z_1 and turns around to enter the U-turn dead zone. After making a U-turn dead zone judgment, the robot stops seeding at Z_2 and completes the U-turn to avoid entering the U-turn dead zone.

2.6.1. Generation of the Boundary Surround Job Path

The U-turns of each parallel work path are collected first, and finally, the meeting point can be formed that can surround the entire boundary, and the vertical axis of each meeting point needs to be accompanied by the corresponding wrapping spacing. Following the parallel work area from starting from the endpoint, the meeting points are connected by polylines in the sequence of ordinal numbers to complete the generation of boundary-wrapping work paths.

2.6.2. Handling of Boundary Surround Paths

There are mainly two optimization methods for the boundary circumnavigation path: one is to directly fit the boundary operation path with a multi-segment line algorithm, and the other is to use the Bézier algorithm to fit and synthesize the boundary curve operation path. By connecting the endpoints of the boundary turning with the polyline algorithm, a series of continuous polyline algorithms are formed. The seeding robot can carry out the sowing operation along a straight line in the polyline algorithm, and the operation is relatively stable.

The Bézier algorithm uses a synthetic curve to drive the chassis in small, smooth curves. The number of right-angle turns can be reduced by fitting multiple segments around the operating path at the boundary. A Bézier curve is a mathematical curve used in two-dimensional graphics applications. Some basic curve definitions include a starting point, an ending point (also known as an anchor point), and the control point. By adjusting the control points, the shape of the Bézier curve changes.

The fitting principle of the Bézier curve is shown in Figure 7. Suppose P_0 , P_0^2 , and P_2 in the figure are three points in a different order on a parabola. The two tangents crossing P_0 and P_2 intersect at P_1 , and the tangents crossing $P_0 P_1$ and $P_2 P_1$ at P_0^2 intersect at P_1^1 and P_1^2 , then the following proportion Equation (7) holds:

$$\frac{P_0 P_0^1}{P_0^1 P_1} = \frac{P_1 P_1^1}{P_1^1 P_2} = \frac{P_0^1 P_0^2}{P_0^2 P_1^1} \quad (7)$$

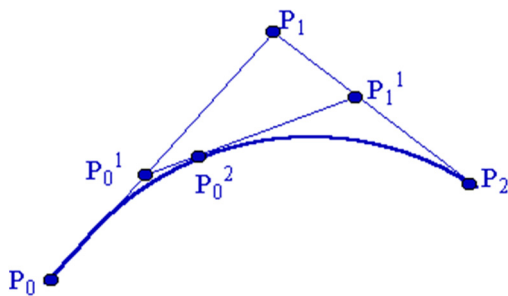


Figure 7. Schematic diagram of Bézier curve fitting.

When $P_{_0}$ and $P_{_2}$ are fixed, the parameter T is introduced to make the above ratio $t:(1 - t)$, that is Equation (8):

$$\begin{aligned} P_0^1 &= (1 - t)P_0 + tP_1 \\ P_1^1 &= (1 - t)P_1 + tP_2 \\ P_0^2 &= (1 - t)P_0^1 + tP_1^1 \end{aligned} \quad (8)$$

When t changes from 0 to 1, the first and second equations in Equation (8) represent the first and second sides of the control bilaterals, respectively, which are two first-order Bézier curves. Substitute the first and second equations in Equation (8) into the third equation to obtain Equation (9):

$$P_0^2 = (1 - t)^2 P_0 + 2t(1 - t)P_1 + t^2 P_2 \quad (9)$$

When t changes from 0 to 1, it represents a quadratic Bézier curve defined via three points: $P_{_0}$, $P_{_1}$, and $P_{_2}$. The quadratic Bézier curve P_0^2 can be defined as a linear combination of a Bézier curve determined by the first two vertices ($P_{_0}$ and $P_{_1}$) and the last two vertices ($P_{_1}$, $P_{_2}$). The cubic Bézier curves are defined by four control points P_0^3 and can be defined as a linear combination of two quadratic Bézier curves determined by ($P_{_0}$, $P_{_1}$, and $P_{_2}$) and ($P_{_1}$, $P_{_2}$, and $P_{_3}$) for $(n + 1)$ control points $P_{_i}$ ($I = 0, 1, \dots, n$). The defined n Bézier curves P_0^n can be defined by the front and rear n control points, respectively, defined by the two $(n - 1)$ times Bézier curves P_1^{n-1} , and the linear combination equation is shown in Equation (10).

$$P_0^n = (1 - t)P_0^{n-1} + tP_1^{n-1}, t \in [0, 1] \quad (10)$$

Thus, the P_i^k is obtained in Equation (11):

$$P_i^k = \begin{cases} P_i, k = 0 \\ \frac{(1 - t)P_i^{k-1} + tP_{i+1}^{k-1}}{(1 - t)P_i^{k-1} + tP_{i+1}^{k-1}}, k = 1, 2, \dots, n; i = 0, 1, \dots, n - k \end{cases} \quad (11)$$

The path planning algorithm in this study is mainly composed of a parallel operation path and boundary surrounding the operation path, and the parallel operation path is to use cyclic detection and pre-collision detection to ensure that the entire map has been traversed. The boundary wrapping path requires supplemental work on the edges of the parallel work area, and the boundary wrapping path is connected by continuous curves or polylines to form a complete wrapping path line. After the operation width is determined, this paper will simulate different strategies and use the polyline algorithm and curve fitting algorithm to solve them, which can be referred to [28–32].

3. Simulation and Experimental Analysis

To verify the feasibility and advantages and disadvantages of the path planning algorithm strategy in seeding operations, this paper combines a simulation test and field verification test. In the simulation experiment, the path planning algorithm used in this paper was compared with the mainstream agricultural path planning algorithm (proposed

algorithm evolutionary hybrid neighborhood search algorithm) and the boundary polylines algorithm for three sets of simulation experiments. In this paper, the name of this path planning algorithm is the improved full coverage algorithm, referred to as the IFC algorithm. The proposed algorithm evolutionary hybrid neighborhood search algorithm is referred to as the EHNS algorithm, the boundary polylines algorithm is referred to as the BP algorithm, and the experimental indicators are coverage, replay rate, curve fitting times, algorithm time, etc.

The whole algorithm process is co-simulated by the mobile-robot-simulator robot in the Intel(R) Core (TM) i5-9300H CPU, 2.40 GHz clock, 12 GB running memory, ROS-kinetic platform (the ROS-kinetic platform is a robotics operating system primarily for Ubuntu 16.04, which uses the programming language C++), path planning algorithm, and tracking-PID robot path tracking. To test the adaptability of the algorithm to the operation of the terraced field seeding robot with different areas and shapes, four irregular real plots of typical hills and mountains with different areas were selected from a terraced field with 666.7 hectares in Sama in Hong He in Yunnan Province, as shown in Figure 8. Boundary data were obtained from Google Earth and derived as KML files. Before the algorithm is called, a Gaussian projection algorithm is used for coordinate transformation, and the GPS coordinates are converted to UTM plane coordinates to obtain a map that can be used for path planning. Then, two working widths are selected for the simulation test. The specific unit parameters are shown in Table 2.

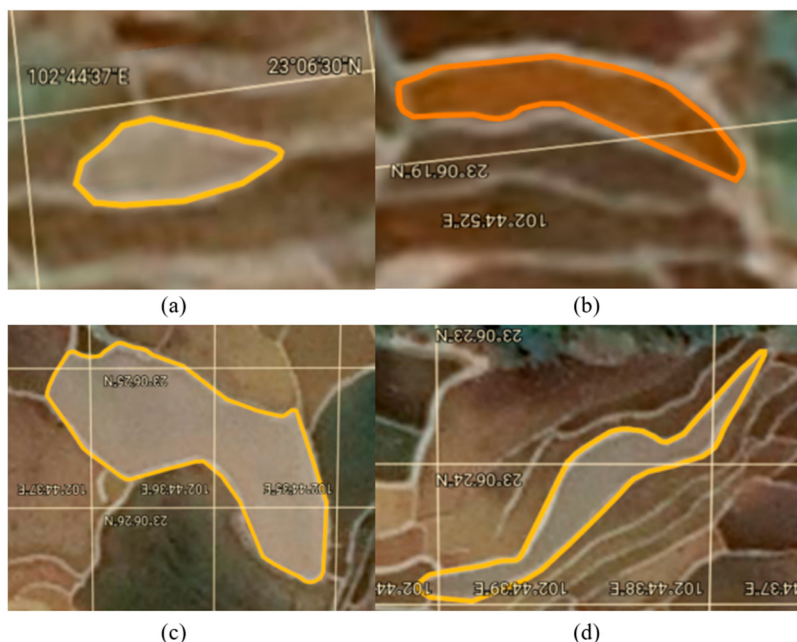


Figure 8. Screenshot of the actual field selected in Google Earth software. (a) Field 1 is small, multilateral, and irregular with an area of 67.94 m²; (b) field 2 is small and irregular, with an area of 87.23 m²; (c) field 3 is large-scale, multilateral and irregular with an area of 1572.97 m²; (d) field 4 is large and irregular with an area of 615.35 m².

Table 2. Unit parameters.

Crew	Number of Work Lines	Length × Height × Width (mm ³)	Working Width (mm)	Minimum Turning Radius (mm)
A	6-row seed metering device	1193 × 699 × 1200	1200	600
B	3-row seed metering device	1193 × 699 × 600	600	300

3.1. The Evaluation Indexes

In addition to the algorithm time, we also need to evaluate the quality of the obtained path. The seeding coverage rate ξ_c and replay rate ξ_d were used to evaluate the operation quality, as shown in Equations (12) and (13).

$$\xi_c = (S_d + S_c)/S_a * 100\% \quad (12)$$

$$\xi_d = (S_{dc} + S_{cc})/S_a * 100\% \quad (13)$$

where S_d is the effective sowing area of the direction parallel area, m^2 , S_c is the effective sowing area of the contour parallel area, m^2 , S_a is the total area of the field to be worked, m^2 , S_{dc} is the repeated sowing area between the direction parallel path sowing area and the contour parallel path sowing area, m^2 , and S_{cc} is the contour parallel path repeating the sowing areas between each other, m^2 .

3.2. Simulation Test Results

Unit B tested small area, irregular fields 1 and 2 of class elliptical shapes, and unit A tested long strips of large, irregular fields 3 and 4. The direction angle of operation was obtained by the maximum span method. The angle with the highest coverage was selected for comparative testing by scheduling the direction of the parallel paths. The linear operation speed was set to 0.5 m/s, the linear backward speed was set to 0.5 m/s, the curve operation speed was set to 0.2 m/s, and the switching time between paths in different states was set to 2 s. The test results are shown in Table 3 and the partial results of the simulation test are shown in Figure 9. In Figure 9, the blue round blocks represent the starting point, and the short, thick, red arrows indicate the initial path direction. The solid yellow line is the boundary line of the field. The dotted magenta line is the parallel operation path line (the magenta arrow is the direction of the parallel operation path). The dotted cyan line is the boundary circumnavigation path line (the cyan arrow is the direction of the boundary circumnavigation path). In the diagram of the replayable operation area, the dark red area represents the replay area, the white area represents the missed area, and the remaining area represents an effective operation area.

Table 3. Irregular field path planning algorithm test results.

Lot No	Unit Number	Algorithm Taken	Number of Fitting Curves	Number of Corners	Repetition Rate (%)	Sowing Coverage (%)	Algorithm CPU-Time (ms)
Field 1	B	EHNS algorithm	/	/	3.02	80.45	12.22
		BP algorithm	0	/116	3.46	95.27	16.41
		IFC algorithm	58	58	3.08	94.45	15.34
Field 2	B	EHNS algorithm	/	/	2.00	79.59	13.53
		BP algorithm	0	126	3.28	94.43	13.87
		IFC algorithm	63	63	2.30	93.53	14.56
Field 3	A	EHNS algorithm	/	/	0.67	80.92	64.66
		BP algorithm	0	52	1.49	95.58	53.94
		IFC algorithm	26	26	1.09	96.30	66.57
Field 4	A	EHNS algorithm	/	/	1.35	78.07	27.65
		BP algorithm	0	62	1.97	94.19	28.03
		IFC algorithm	31	31	1.51	96.45	30.22

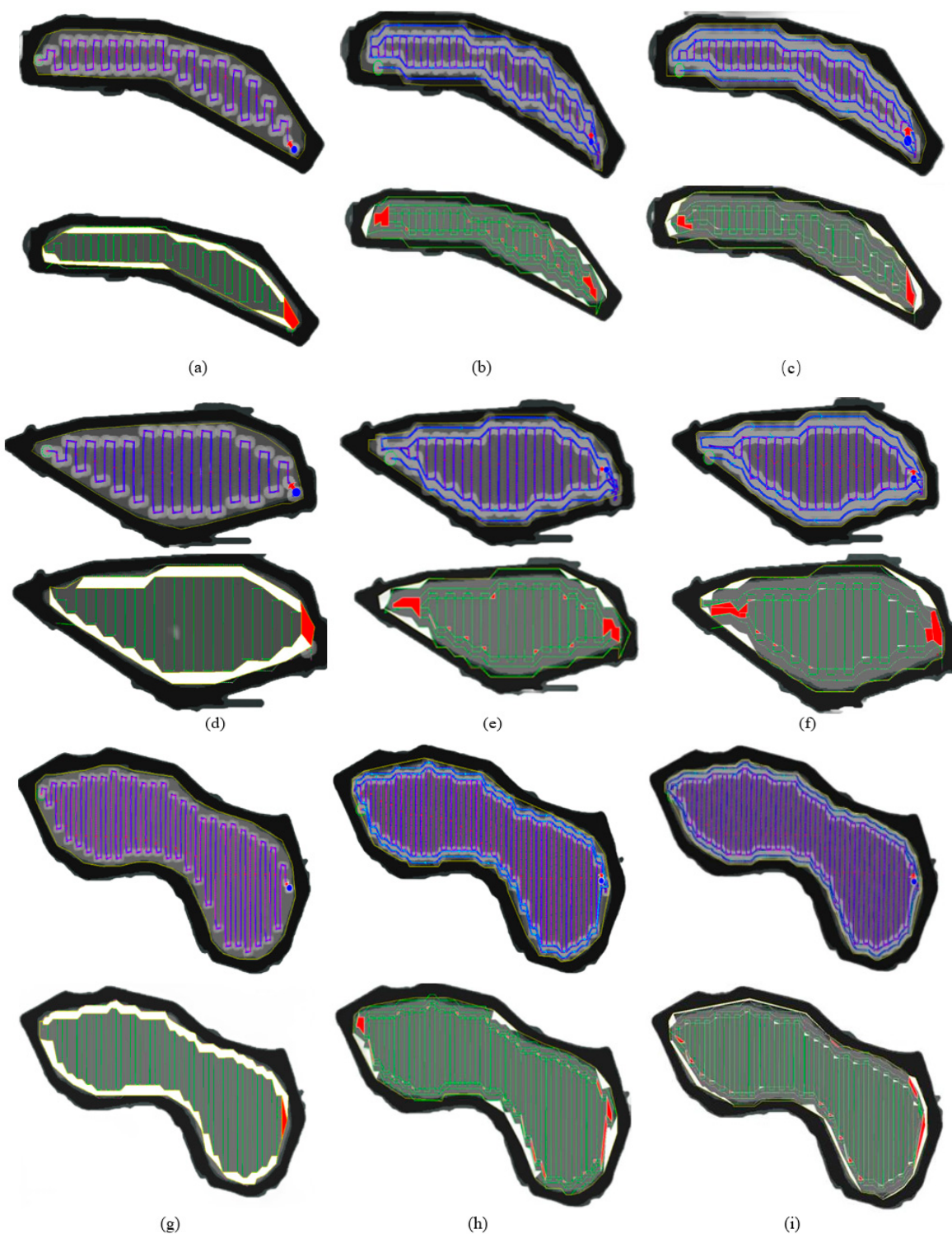


Figure 9. *Cont.*

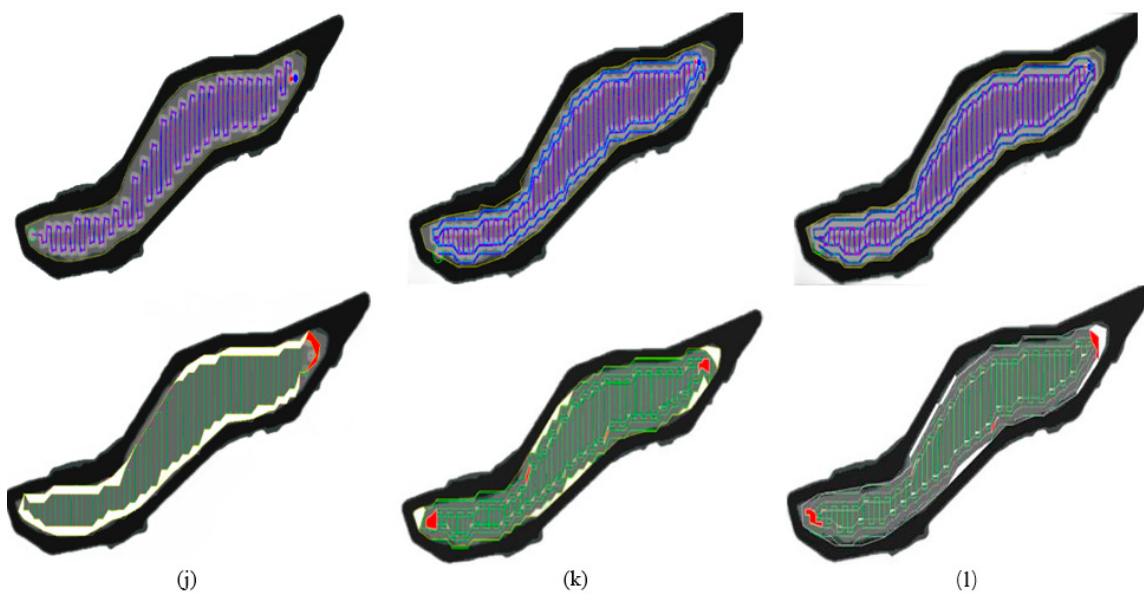


Figure 9. Screenshot of the calculation example results for irregular fields. (a) B-field 1 path planning simulation and replay evaluation of the EHNS algorithm; (b) B-field 1 path planning simulation and replay evaluation of the BP algorithm; (c) B-field 1 path planning simulation and replay evaluation of the IFC algorithm; (d) B-field 2 path planning simulation and replay evaluation of the EHNS algorithm; (e) B-field 2 path planning simulation and replay evaluation of the BP algorithm; (f) B-field 2 path planning simulation and replay evaluation of the IFC algorithm; (g) A-field 3 path planning simulation and replay evaluation of the EHNS algorithm; (h) A-field 3 path planning simulation and replay evaluation of the BP algorithm; (i) A-field 3 path planning simulation and replay evaluation of the IFC algorithm; (j) A-field 4 path planning simulation and replay evaluation of the EHNS algorithm; (k) A-field 4 path planning simulation and replay evaluation of the BP algorithm; (l) A-field 4 path planning simulation and replay evaluation of the IFC algorithm.

In Figure 9, through the brief analysis of the simulation results of seeding robot operation in irregular boundary fields in hilly and mountainous areas, the average coverage of the EHNS algorithm is 79.75%, the average coverage of the BP algorithm is 94.86%, and the average coverage of the IFC algorithm is 95.20%. Therefore, in terms of coverage, the BP algorithm and the IFC algorithm using the parallel job path + boundary surround path strategy are significantly higher than the EHNS algorithm using only the parallel job path strategy. The IFC algorithm using curve fitting for the boundary wrapping path is slightly higher than the BP algorithm using polyline for the boundary wrapping path, indicating that the path strategy using parallel operation path + boundary wrapping curve fitting has improved the coverage to a certain extent.

3.3. Validation Tests and Analysis of the Results

The plot of the verification test is located in the Cen Village Teaching and Experimental Base of South China Agricultural University, Tianhe District, Guangzhou, Guangdong Province, China, with no internal obstacles, and the inside of the plot is divided into four plots numbered 1, 2, 3 and 4 for the simulation of the four Yunnan Hong He terraces used in the simulation test. The field verification test of path planning was carried out according to the number, the plot outline, and the specific information of the test plot as shown in Figure 10, and the test time is November 2022.

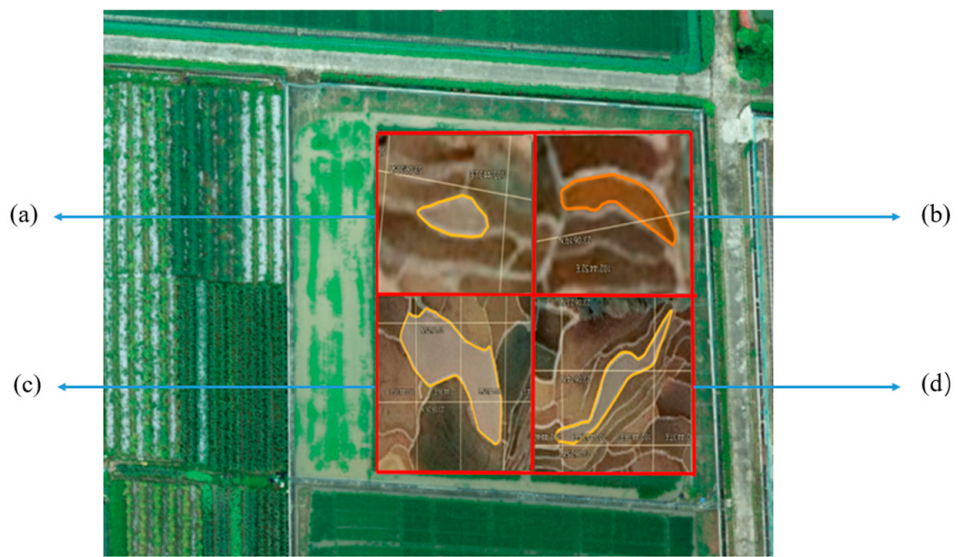


Figure 10. The profile and number of the field block of the verification test. (a) represents the field block that simulates the outline of field block 1; (b) represents the plot that simulates the contour of field block 2; (c) represents a plot that simulates the contour of plot 3; and (d) represents a plot that simulates the contour of plot 4.

The verification test platform in this paper is a four-wheel differential chassis with a navigation function; the test platform is based on Song-Ling SCOUT2.0 chassis. By fusing the GPS position information and the heading angle information of the dual-antenna Sinan M600mini, the navigation algorithm of the chassis is independently written. The robot chassis can perform path tracking, speed control, position acquisition, and other functions; the robot chassis is shown in Figure 11.



Figure 11. Actual picture of the seeding robot. (a) denotes the dual-antenna GNSS; (b) indicates the industrial computer screen; (c) indicates the industrial computer; and (d) indicates the robot chassis.

To verify the sowing path planning of the four plots tested in the simulation experiment, the path planning of the four plots in the simulation experiment was used as the path planning reference, the path planning and tracking were carried out by using the seeding robot chassis, and the coverage and replay rate of the four plots were counted. The analysis of the results of the field validation test is shown in Table 4.

Table 4. Validation of the test results of the experiment.

Block Number	Total Area/ m ²	Missed Area/ m ²	Repetition Area/ m ²	Coverage/%	Repetition Rate/%
1	67.94	3.41	1.22	94.97	1.80
2	87.23	4.94	1.75	94.33	2.01
3	1572.97	39.48	47.66	97.49	3.03
4	615.35	33.16	16.61	94.61	2.70

The test results of path planning verification are divided into a reference planning path and an actual path; the reference planning path is generated by the imported field map, starting point, operation direction, and robot radius, and the actual path is obtained by continuously recording the trajectory points of robot navigation. In the path planning results of Figure 12, the solid light blue line represents the actual trajectory of the robot, the red dashed line represents the reference path plan, and the magenta fence line represents the farmland boundary.

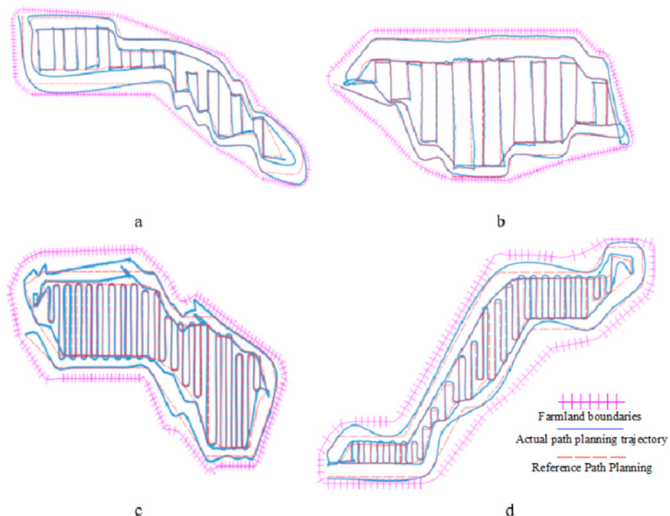


Figure 12. Verification of the path trace results for the experiment. (a) represents the path tracking result of field block 1; (b) represents the path tracking result of field block 2; (c) represents the path tracking result of field block 3; and (d) represents the path trace result of field block 4.

In the path tracking data of the Figure 11 verification test, the current real-time lateral deviation is calculated by comparing the GPS path planning reference point with the actual trajectory point recorded by the GPS. By comparing the GPS reference heading with the actual heading recorded by the GPS, the current real-time heading deviation is calculated, and the lateral deviation and heading deviation data for each field plot are shown in Table 5.

Table 5. Verification test for the lateral deviation and heading deviation statistics.

Block Number	Maximum Lateral Deviation/mm	Average Lateral Deviation/mm	Maximum Heading Deviation/rad	Average Heading Deviation/rad
1	11	4.4	0.082	0.069
2	9.9	4.7	0.091	0.087
3	8.6	4.5	0.077	0.070
4	9.7	5.3	0.080	0.066

In the replay and missed evaluation in Figure 13, the solid blue line represents the farmland boundary, the yellow area represents the missed area, and the red area represents the replay area.

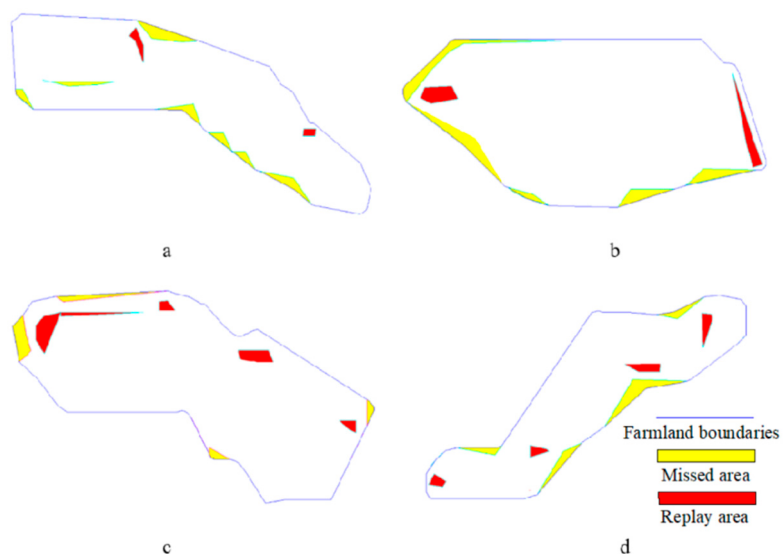


Figure 13. Validation of the replay and missed area. (a) Field Block 1; (b) field block 2; (c) field block 3; (d) field block 4.

4. Discussion

Through the simulation test results of the seeding robot's operation in irregular boundary fields in hilly and mountainous areas, the algorithm has good adaptability to typical irregular fields and can meet the requirements of irregular boundary field seeding robots for operation path planning. The coverage rate can reflect the ratio of the sown area to the missed area of the path planning algorithm in the actual production test, and the higher the coverage, the higher the benefit brought by seeding. For the EHNS algorithm, through the simulation test of four types of typical fields in hilly and mountainous areas, the coverage rate of the fields was 78.07~80.92%. For the BP algorithm, through the simulation test of four types of typical fields in hilly and mountainous areas, the coverage rate of the plots was 94.16~95.58%. For the IFC algorithm used in this paper, through the simulation test and field verification test of four types of typical fields in hilly and mountainous areas, the coverage rate of the fields was 93.53~96.54%. The field verification test showed that the coverage rate of the plot was 94.33~97.49%. Therefore, the parallel operation path + boundary wrapping path algorithm of the IFC algorithm is more successful in coverage, which can improve the coverage of field path planning to a certain extent.

Repetition leads to the waste of seeds, fertilizers, fuel, etc., so it is necessary to reduce the repetition rate as much as possible under certain conditions. For the EHNS algorithm, through the simulation test of four types of typical fields in hilly and mountainous areas, the repetition rate of the fields was 0.67~3.46%. For the BP algorithm, through the simulation test of four types of typical fields in hilly and mountainous areas, the repetition rate of the plots was 1.49~3.08%. For the IFC algorithm used in this paper, through the simulation test and field verification test of four types of typical fields in hilly and mountainous areas, the repetition rate of the field plot was 1.09~3.08%. The field verification test showed that the repetition rate of the field plot was 1.80~3.03%. According to China's technical specifications for sowing quality evaluation, the refill rate in a field is less than 15% to meet the technical requirements, so the IFC algorithm used in this paper—as well as the EHNS and the BP algorithms—meet the practical application requirements of agricultural production.

There are two measures selected for the boundary wrapping operation path: one is that the boundary is connected around the polyline, the other is that the boundaries are connected around curves. These two measures have their advantages and disadvantages; the boundary is connected around the polyline, which will reduce the complexity of the algorithm and have high operational efficiency, but it is easy to cause the robot's seeding path to deviate, thereby affecting the seeding quality. The boundary is connected around the curve, and the polyline will be fitted, which reduces the number of robot corner turns,

improves the seeding quality, and improves the smoothness of the path, but the algorithm requires a large operation and high complexity. Through the comparison test between the IFC algorithm and BP algorithm, the number of fitting turns and the number of corner turns of the BP algorithm were compared with the test indicators, and the number of curve fitting turns of the BP algorithm was less than that of the IFC algorithm, and the number of a corner turns of the BP algorithm was half that of the IFC algorithm. Therefore, the boundary is curved around the working path to fit the curve, so that the robot travels along the curve while working, which can reduce the inertia caused by large turns, and the seeding will be more uniform. Moreover, the difference in the algorithm CPU time between the two algorithms is within 20 ms, which shows the efficiency and stability of the algorithm.

5. Conclusions

Aimed at the problem of full-coverage sowing path planning of irregular fields in hilly and mountainous areas, combined with the typical characteristics of different areas, shapes, and boundaries of hilly terraces, a method of operation path planning based on the combination of parallel operation and boundary encirclement operation is proposed, and tests were carried out by combining a simulation test and a field verification test, and the field verification test results are in high agreement with the simulation test results, indicating that the path planning algorithm adopted in this paper has good adaptability and stability.

By comparing the IFC path planning algorithm with the mainstream agricultural path planning algorithm EHNS, the plot coverage of the parallel operation path + boundary surrounding operation path strategy is always greater than that of the traditional EHNS algorithm strategy, indicating that the algorithm has good adaptability in improving the coverage of irregular field path planning.

By comparing the IFC path planning algorithm with the BP path planning algorithm in this study, the multi-segment line boundary surrounding the operation path is directly connected by the multi-segment line. So that the corner turning amplitude of the boundary wrap is large and the seeding is uneven, we optimized the boundary wrapping operation path and used the Bézier curve fitting method to fit the original multi-segment polyline into a multi-segment curve, which can help improve the accuracy of robot seeding and the stability of driving.

To verify the feasibility of the path planning algorithm, this paper adopts a test method combining a simulation test and a field test, and the simulation test was carried out in July 2022 and the field verification test was carried out in November 2022. Through the analysis of the results of the simulation test and the field verification test, the verification test results and the simulation test results are consistent, the coverage rate is greater than 95.00%, and the replay rate is less than 4.00%. This shows that the path planning algorithm adopted in this paper has good adaptability to irregular fields in practical applications, and the coverage and replay rate are in line with the production requirements of rice sowing.

Although the path planning of the seeding robot generated by this research method has good performance in the coverage and replay rates of irregular fields, the number of turns of parallel operation path planning in this path planning is still too much, which will increase energy consumption and reduce operation.

6. Patents

There is a Chinese invention patent resulting from the work reported in this manuscript; its patent name is “A path planning method for complex boundary farmland and farmland machine operating system” and its patent publication number is CN114839976A.

Author Contributions: Conceptualization: W.Y., C.G. and Y.Z.; writing—original draft preparation: C.G., W.Y. and J.H.; writing—review and editing: X.L., E.C., S.S., C.G., W.Y. and W.C.; methodology: C.G. and Y.Z.; visualization: C.G. and H.X.; supervision: C.G. and W.Y. All authors have read and agreed to the published version of the manuscript.

Funding: This research received no external funding.

Acknowledgments: The authors gratefully acknowledge financial support from Special Projects in the National Key R&D Program of China (2021YFD2000405-4), the key area of “Artificial Intelligence” of General Colleges and Universities in Guangdong Province (2019KZDZX1003), and Independent Research and Development Projects of Maoming Laboratory (2021ZZ001).

Conflicts of Interest: The authors declare no conflict of interest. The funders had no role in the design of the study; in the collection, analysis, or interpretation of the data; in the writing of the manuscript; or in the decision to publish the results.

References

- Hui, X.; Sun, Y.; Yin, F.; Dun, W. Trend Prediction of Agricultural Machinery Power in China Coastal Areas Based on Grey Relational Analysis. *J. Coast. Res.* **2020**, *103*, 299. [[CrossRef](#)]
- Liu, S.-Q.; Zhang, H.-Q.; Xie, F.-T.; Guo, S.-L. Current situation and influencing factors of pluriactivity in mountainous and hilly rural areas of Sichuan province, China. *J. Mt. Sci.* **2013**, *10*, 445–454. [[CrossRef](#)]
- Yang, M.; Li, M.; Luo, X. 50 Years of Agricultural Mechanization in China. *Ama-Agric. Mech. Asia Afr. Lat. Am.* **2020**, *51*, 86–92.
- Cong, C. Research on mechanized production technology mode of rice in the hilly and mountainous areas of southern China. *China Master's E-J.* **2012**, *10*, 79.
- Ranou, G. Reflections on the development of agricultural mechanization in the hilly and mountainous areas of southern China. *Rural. Econ. Sci. Technol.* **2017**, *28*, 196–197.
- Xiaofeng, H. Problems and suggestions for the development of agricultural mechanization in hilly and mountainous areas. *China Agric. Mach. Superv.* **2021**, *6*, 45–46.
- Jin, Y.; Liu, J.; Xu, Z.; Yuan, S.; Li, P.; Wang, J. Development status and trend of agricultural robot technology. *Int. J. Agri-Cult. Biol. Eng.* **2021**, *14*, 1–19. [[CrossRef](#)]
- Qi, R. Mechanization transformation in hilly and mountainous areas promotes the construction of agricultural standardization. *China's Agric. Dev. Equip.* **2020**, *8*, 128.
- Weiwei, W.; Liqing, C.; Yang, Y.; Lichao, L. Development and Prospect of Agricultural Machinery Chassis Technology. *Trans. Chin. Soc. Agric. Mach.* **2021**, *52*, 1–15.
- Feng, Q.; Zou, W.; Fan, P.; Zhang, C.; Wang, X. Design and test of robotic harvesting system for cherry tomato. *Int. J. Agric. Biol. Eng.* **2018**, *11*, 96–100. [[CrossRef](#)]
- Leu, A.; Razavi, M.; Langstädler, L.; Ristic-Durrant, D.; Raffel, H.; Schenck, C.; Graser, A.; Kuhfuss, B. Robotic Green Asparagus Selective Harvesting. *IEEE/ASME Trans. Mechatron.* **2017**, *22*, 2401–2410. [[CrossRef](#)]
- Kim, J.-S.; Ju, Y.-T.; Kon, K. Object Recognition Technology using LiDAR Sensor for Obstacle Detection of Agricultural Autonomous Robot. *J. Korea Inst. Electron. Commun. Sci.* **2021**, *16*, 565–570.
- Luo, X.; Wang, Z.; Zeng, S.; Zang, Y.; Yang, W.; Zhang, M. Recent advances in mechanized direct seeding technology for rice. *J. South China Agric. Univ.* **2019**, *40*, 1–13.
- Wei, L. Research on key technologies of cucumber picking robots. *China Master's E-Journal*.
- Runxin, N.; Xiangyang, Z.; Jie, W.; Hui, Z.; Huang, J.; Chen, Z. Orchard Trunk Detection Algorithm for Agricultural Robot Based on Laser Radar. *Trans. Chin. Soc. Agric. Mach.* **2020**, *51*, 21–27.
- Zekuan, L. Thinking and countermeasures for the development of agricultural mechanization in hilly and mountainous areas. *Chin. Agric. Mach.* **2010**, *14*, 9–11.
- Cabreira, T.M.; Brisolara, L.B.; Ferreira, P.R., Jr. Survey on Coverage Path Planning with Unmanned Aerial Vehicles. *Drones* **2019**, *3*, 4. [[CrossRef](#)]
- Galceran, E.; Carreras, M. A survey on coverage path planning for robotics. *Robot. Auton. Syst.* **2013**, *61*, 1258–1276. [[CrossRef](#)]
- Jensen, M.A.F.; Bochtis, D.; Sørensen, C.G.; Blas, M.R.; Lykkegaard, K.L. In-field and inter-field path planning for agricultural transport units. *Comput. Ind. Eng.* **2012**, *63*, 1054–1061. [[CrossRef](#)]
- Chakraborty, S.; Elangovan, D.; Govindarajan, P.L.; ELNaggar, M.F.; Alrashed, M.M.; Kamel, S. A Comprehensive Review of Path Planning for Agricultural Ground Robots. *Sustainability* **2022**, *14*, 9156. [[CrossRef](#)]
- Utamima, A.; Reiners, T.; Ansari-poor, A.H. Optimisation of agricultural routing planning in field logistics with Evolutionary Hybrid Neighbourhood Search. *Biosyst. Eng.* **2019**, *184*, 166–180. [[CrossRef](#)]
- Oksanen, T.; Visala, A. Coverage path planning algorithms for agricultural field machines. *J. Field Robot.* **2009**, *26*, 651–668. [[CrossRef](#)]
- Kiani, F.; Seyyedabbasi, A.; Nematzadeh, S.; Candan, F.; Çevik, T.; Anka, F.A.; Randazzo, G.; Lanza, S.; Muzirafuti, A. Adaptive Metaheuristic-Based Methods for Autonomous Robot Path Planning: Sustainable Agricultural Applications. *Appl. Sci.* **2022**, *12*, 943. [[CrossRef](#)]
- Jin, J.; Tang, L. Optimal Coverage Path Planning for Arable Farming on 2D Surfaces. *Trans. ASABE* **2010**, *53*, 283–295. [[CrossRef](#)]
- Kai, C.; Mountain, X.; Yanming, L.; Chengliang, L. Full Coverage Path Planning Method of Agricultural Machinery under Multiple Constraints. *Trans. Chin. Soc. Agric. Mach.* **2022**, *53*, 17–26+43.

26. Ruyue, C.; Zhenqian, Z.; Shichao, L.; Man, Z. Multi-machine Cooperation Global Path Planning Based on A-star Algorithm and Bezier Curve. *Trans. Chin. Soc. Agric. Mach.* **2021**, *52*, 548–554.
27. Xiaomao, H.; Lei, Z.; Shaoshuai, W.; Chengming, L. Path Planning of Rapeseed Combine Seeder in Field of Convex Boundary. *Trans. Chin. Soc. Agric. Mach.* **2022**, *53*, 33–40+150.
28. Azevedo, L.G.; Monteiro, R.S.; Zimbrão, G.; De Souza, J.M. Polyline Spatial Join Evaluation Using Raster Approximation. *Geoinformatica* **2003**, *7*, 315–336. [[CrossRef](#)]
29. Chen, X.-D.; Yang, C.; Ma, W. Coincidence condition of two Bézier curves of an arbitrary degree. *Comput. Graph.* **2016**, *54*, 121–126. [[CrossRef](#)]
30. Eze, M.; Okunbor, C.; Aleburu, D.; Adekola, O.; Ramon, I.; Richard-Nnabu, N.; Avwokuruaye, O.; Olayiwola, A.; Yoro, R.; Solomon, E. Graphics Evolutionary Computations in Higher Order Parametric Bezier Curves. *Comput. Syst. Sci. Eng.* **2022**, *41*, 595–609. [[CrossRef](#)]
31. Gribov, A.; Bodansky, E. A new method of polyline approximation. In Proceedings of the Structural, Syntactic, and Statistical Pattern Recognition: Joint IAPR International Workshops, SSPR 2004 and SPR 2004, Lisbon, Portugal, 18–20 August 2004; Springer: Berlin/Heidelberg, Germany, 2004; pp. 504–511. [[CrossRef](#)]
32. Yan, L.; Liang, J. An extension of the Bezier model. *Appl. Math. Comput.* **2011**, *218*, 2863–2879. [[CrossRef](#)]

Disclaimer/Publisher's Note: The statements, opinions and data contained in all publications are solely those of the individual author(s) and contributor(s) and not of MDPI and/or the editor(s). MDPI and/or the editor(s) disclaim responsibility for any injury to people or property resulting from any ideas, methods, instructions or products referred to in the content.